Chinese Chemical Letters 34 (2023) 107771

Contents lists available at ScienceDirect

Chinese Chemical Letters

journal homepage: www.elsevier.com/locate/cclet

# A new semiconductor-based SERS substrate with enhanced charge collection and improved carrier separation: CuO/$TiO_2$ p-n heterojunction

Dongxue Yu [a], Lin Xu [a], Huizhu Zhang [a], Jia Li [a], Weie Wang [a], Libin Yang [a,*], Xin Jiang [a,*], Bing Zhao [b,*]

[a] College of Materials Science and Engineering, College of Pharmacy, Jiamusi University, Jiamusi 154007, China
[b] State Key Laboratory of Supramolecular Structure and Materials, Jilin University, Changchun 130012, China

ARTICLE INFO

*Article history:*
Received 30 June 2022
Revised 22 July 2022
Accepted 20 August 2022
Available online 23 August 2022

*Keywords:*
SERS
CuO/$TiO_2$ heterojunction
Photo-induced charge transfer
Semiconductor substrate
Charge collection
Carrier separation

ABSTRACT

In this paper, CuO/$TiO_2$ p-n heterojunction was developed as a new surface enhanced Raman scattering (SERS) substrate to magnify Raman signal of 4-mercaptobenzoic acid (4-MBA) molecule. In the heterojunction-molecule system, CuO as an "electron capsule" can not only offer more electrons to inject into the surface state energy level of $TiO_2$ and consequently bring additional charge transfer, but also improve photogenerated carrier separation efficiency itself due to strong interfacial coupling in the interface of heterojunction, which together boost SERS performance of the heterojunction substrate. As expected, owing to the enhanced charge collection capacity and the improvement of photogenerated carrier separation efficiency derived from internal electric field and strong interface coupling provided in the interface of heterojunction, this substrate exhibits excellent SERS detection sensitivity towards 4-MBA, with a detection limit as low as $1 \times 10^{-10}$ mol/L and an enhancement factor of $8.87 \times 10^6$.



Surface enhanced Raman scattering (SERS) technology, characterized by nondestructive detection and ultrahigh single-molecular sensitivity etc., has attracted great attention in the fields of biosensor, photocatalysis, trace detection, chemical analysis and virus detection [1–6]. Development of SERS as a surface enhancement technology depends on the exploitation of substrate materials. The noble metal materials (such as Au, Ag) as the traditional substrates can provide highly SERS enhancement factors (EFs) of $10^6$–$10^{10}$ due to its localized surface plasmon resonance (LSPR) effect [7]. However, there are still inevitable disadvantages, such as high cost, limited types, poor uniformity and stability [8,9]. By comparison, semiconductor substrates have some inherent advantages of lower cost, richer types, higher stability, better biocompatibility, tunable properties and selective enhancement of molecular Raman signals [10,11]. Regrettably, one bottleneck problem of semiconductor-based SERS substrate is that the EFs are lower compare to noble metal substrate, which hinders its practical application [12].

The enhancement mechanism of semiconductors can be attributed to the photo-induced charge transfer (PICT) between the substrate and the target molecule. When the probe molecule is adsorbed on the semiconductor substrate, the strong PICT will effectively increase the scattering volume and the polarizability of the probe molecule, so as to obtain larger Raman scattering cross-sectional area and stronger Raman signal of molecule [13]. Thus, how to enhance and promote PICT efficiency of semiconductor nanomaterials by means of effective tuning strategies is a key issue for the development of high-performance semiconductor SERS substrate.

Some strategies have been developed in semiconductor-molecule systems. Zhao's group effectively promoted the PICT resonance by tuning the oxygen element content or surface defect in the semiconductor substrate (oxygen-doped $MoS_2$, oxygen-deficient $W_{18}O_{49}$ or $WO_3$ nanosheet) [9,14,15]. Guo *et al.* indicated that introducing the amorphous structure into two-dimensional $TiO_2$ nanosheet could greatly narrowed the band gap of $TiO_2$ substrate, which effectively promoted the PICT resonance [16]. Recently, our group finds that some metal-doped semiconductors can promote the PICT resonance in the substrate-molecule system by doping energy levels between conduction band (CB) and the valence band (VB) of semiconductors, which play a role similar to surface state energy level ($E_{ss}$) [17–20]. The above researches indicated that adjusting the energy band structure or electron con-

* Corresponding authors.
*E-mail addresses:* yanglibin@jmsu.edu.cn (L. Yang), jiangxin@jmsu.edu.cn (X. Jiang), zhaob@mail.jlu.edu.cn (B. Zhao).

https://doi.org/10.1016/j.cclet.2022.107771
1001-8417/

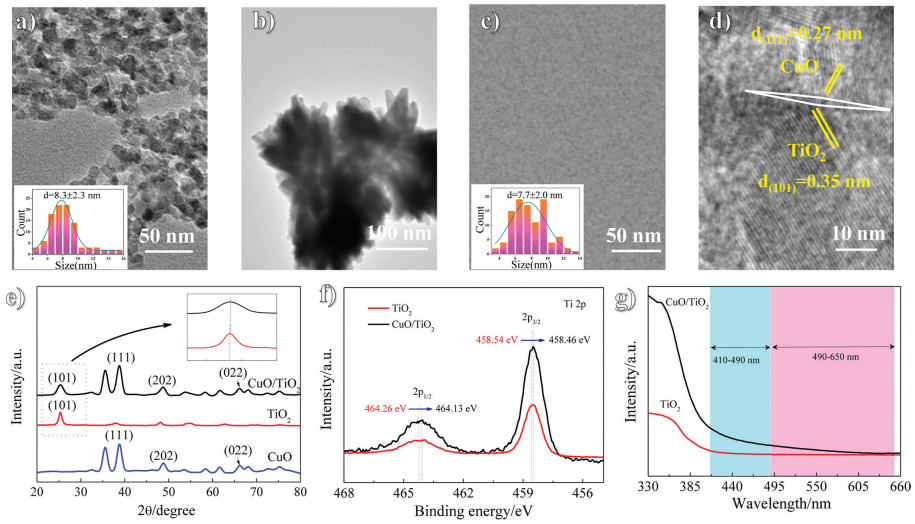


**Fig. 1.** TEM images of (a) $TiO_2$, (b) CuO, (c) $CuO/TiO_2$ heterojunction. Insets of (a) and (c) are the corresponding size distribution histograms of $TiO_2$ and $CuO/TiO_2$ heterojunction. (d) HRTEM of $CuO/TiO_2$ heterojunction. (e) XRD patterns of $TiO_2$, CuO and $CuO/TiO_2$ heterojunction. (f) High-resolution XPS spectra of Ti 2p of $TiO_2$ and $CuO/TiO_2$ heterojunction. (g) UV–vis DRS of $TiO_2$ and $CuO/TiO_2$ heterojunction.

figuration of single semiconductor can be regarded as an effective strategy to promote PICT resonance. However, the tuning for the semiconductor itself or intrinsic electronic structure (defects) is also limited, which often ignores the important effects of concentration and recombination of photogenerated carriers on PICT and SERS. Based on PICT enhancement mechanism, increasing the concentration and separation efficiency of photogenerated carriers should be other effective strategies for the development of new semiconductor SERS substrates with high EF.

Semiconductor heterojunction is a kind of semiconducting structure, which is formed by the combination of two different semiconductor materials. The heterojunction composed of wide-band gap semiconductor and narrow-band gap semiconductor, especially p-n type heterojunction, can extend the light response range and consequently result in generation of large-scale separable electron hole pairs [21–23], which increases the possibility of electronic transition. In addition, the heterojunction is also an available structure for significantly enhancing the separation and transfer of photogenerated carriers due to the formation of band bending and internal electric field (IEF) at the interface of heterojunction. Thus, the interface engineering should be an idea and effective method for the design and construction of high-performance semiconductor SERS substrate.

Here, we take $CuO/TiO_2$ heterojunction as an example to explore the feasibility of p-n heterojunction as a high-performance SERS substrate based on the interface engineering strategy. As expected, $CuO/TiO_2$ heterojunction exhibits excellent SERS performance for probe molecule (4-mercaptobenzoic acid, 4-MBA) with a low limit of detection (LOD) of $1 \times 10^{-10}$ mol/L and a high EF of $8.87 \times 10^6$. The excellent SERS performance can be attributed to the enhanced charge collection capacity and the improvement of photogenerated carrier separation efficiency derived from the internal structure of heterojunction, which effectively enhances and promotes PICT.

In this work, CuO was synthesized by chemical precipitation method and then served as a precursor to add into the sol-hydrothermal synthesis system of $TiO_2$ for further preparation of $CuO/TiO_2$ heterojunction. For comparison, pure CuO and $TiO_2$ were synthesized at the same time. In order to confirm the type of semiconductor (CuO, $TiO_2$) and the construction of p-n junction, the Mott-Schottky (MS) measurements of samples were carried out. As shown in Fig. S1 (Supporting information), CuO shows a negative slope (Fig. S1a), while $TiO_2$ shows a positive slope (Fig. S1b), indicating that CuO is a p-type semiconductor and $TiO_2$ is an n-type semiconductor. Differently, in $CuO/TiO_2$ heterojunction, the slope of MS plots below −0.3 V *vs.* Ag/AgCl is negative while that above −0.3 V is positive (Fig. S1c), which is in accordance with the reported typical "V-shaped" MS plots of p-n junctions [24] and thus provides a solid foundation for the presence of p-n junction. Morphology of the samples is characterized by transmission electron microscope (TEM). Pure $TiO_2$ shows a spherical structure with a diameter of $8.3 \pm 2.3$ nm (Fig. 1a). Pure CuO has ultra-fine structure, which looks like a structure similar to "Chinese ink painting" composed of ultra-fine particles (Fig. 1b). For $CuO/TiO_2$ heterojunction, it can be clearly observed that CuO nanoparticles (NPs) are dispersed on the surface of $TiO_2$ NPs, and the average grain size of $TiO_2$ NPs ($7.7 \pm 2.0$ nm) decreases compared with that of pure $TiO_2$ (Fig. 1c), which is attributed to the inhibition of CuO on the growth of $TiO_2$ grains. In the high resolution transmission electron microscope (HRTEM) of the heterojunction (Fig. 1d), a closely interface heterostructure is observed between CuO and $TiO_2$. The lattice spacing values are 0.35 and 0.27 nm, which are corresponded to the (101) plane of anatase $TiO_2$ and the (111) plane of monoclinic CuO nanocrystals, respectively.

Fig. 1e shows the X-ray diffraction (XRD) patterns of $TiO_2$, CuO and $CuO/TiO_2$ heterojunction. The diffraction peaks of the pure $TiO_2$ NPs are highly matched within anatase $TiO_2$ (JCPDS No. 21–1272) [25,26]. The peaks of CuO NPs at 25.16°, 38.8°, 48.7°and 66.2° are assigned to (002), (111), (202) and (022) crystal planes of monoclinic CuO structure (JCPDS No. 00–002–1040) [27]. $CuO/TiO_2$ sample shows all characteristic peaks of anatase $TiO_2$ and monoclinic CuO structure, indicating the successful formation of heterojunction composite. It should be noted that the position of anatase (101) peak in the $CuO/TiO_2$ heterojunction shifts to higher $2\theta$ value (25.4°) compared with that (25.3°) of pure $TiO_2$ (inset Fig. 1e), which indicates that Cu was incorporated into the $TiO_2$ lattice [28]. Furthermore, the (101) diffraction peak is broadened compared to that of pure $TiO_2$. It means that the degree of crystallinity of $TiO_2$ component in the heterojunction as well as crystallite size decreases, which is consistent with TEM result.

X-ray photoelectron spectrum (XPS) measurements were carried out to confirm the element composition and chemical state of $CuO/TiO_2$ heterojunction. The XPS survey spectrum clearly suggested that there are Ti, Cu and O elements coexisting in the

$CuO/TiO_2$ heterojunction (Fig. S2a in Supporting information). The high resolution Cu 2p peak of heterojunction can be fitted into two peaks arising from Cu $2p_{1/2}$ and Cu $2p_{3/2}$ orbitals located at 954.6 and 934.5 eV (Fig. S2b in Supporting information), suggesting that Cu exists in the sample in the form of +2 oxidation state [29,30]. The Ti 2p XPS spectra of $TiO_2$ and $CuO/TiO_2$ heterojunction are displayed in Fig. 1f. For the $TiO_2$ sample, the peaks positioned at 458.54 and 464.26 eV are corresponding to the Ti $2p_{3/2}$ and Ti $2p_{1/2}$ of $Ti^{4+}$. Compared with pure $TiO_2$, the Ti $2p_{3/2}$ and Ti $2p_{1/2}$ peaks of $CuO/TiO_2$ heterojunction shift 0.08 and 0.13 eV toward lower binding energy, respectively. The similar case can also be seen in the O 1s XPS spectra, in which the O 1s peak (531.54 eV) of $CuO/TiO_2$ shifts to a lower binding energy compared with that (531.45 eV) of pure $TiO_2$ (Fig. S2c in Supporting information). These indicate a higher electron density of the Ti and O atoms in the $CuO/TiO_2$ heterojunction. This can be attributed to the formation of Ti-O-Cu bonds due to the introduction of CuO.

The UV–vis diffuse reflectance spectra (DRS) of $TiO_2$ and $CuO/TiO_2$ heterojunction samples were shown in Fig. 1g. The photoabsorption of pure $TiO_2$ NPs was observed at 330–410 nm, which can be attributed to the band-band electron transition according to its band gap energy. The tailing in the region of 410–490 nm corresponds to the photoabsorption related to $E_{ss}$ of the $TiO_2$ NPs (*i.e.*, blue region). Compared with pure $TiO_2$ NPs, the heterojunction sample exhibits a wider range of photoabsorption in the range of 410–650 nm, which is ascribed to the band-band electron transition of CuO in the heterojunction.

The SERS performances of the substrates were assessed using the 4-MBA molecule as Raman reporter. Fig. 2a shows the SERS spectra of 4-MBA ($10^{-3}$ mol/L) adsorbed on the surface of pure $TiO_2$, pure CuO, mixture of $TiO_2$ and CuO and $CuO/TiO_2$ heterojunction. As expected, $CuO/TiO_2$ heterojunction shows superior SERS enhancement compared with other substrates (the specific assignments of SERS peak for 4-MBA on substrate are listed in Table S1 in Supporting information). Take the peak at 1594 $cm^{-1}$ as an example, the SERS enhancement intensity on the heterojunction is about 8.61 and 4.09 times larger than those on the pure $TiO_2$ NPs and mixture of $TiO_2$ and CuO NPs, respectively (Fig. 2b). However, the SERS signal of 4-MBA molecule on CuO NPs was not even observed. Obviously, the excellent SERS performance of $CuO/TiO_2$ p-n heterostructure must be derived from the strong interface coupling in heterojunction. It is further verified by the fact that SERS enhancement of the mixture is significantly weaker than that of the heterojunction, while slightly higher than that of the pure $TiO_2$, which can be attributed to the weak interaction between CuO and $TiO_2$ in the mixture.

For further understanding the SERS enhancement mechanism and revealing the role of heterojunction in the PICT process, the energy level position of $CuO/TiO_2$-molecule system was given in Fig. 2c according to the VB and CB positions of semiconductors (CuO and $TiO_2$), the lowest unoccupied molecular orbital (LUMO) and the highest occupied molecular orbital (HOMO) positions of 4-MBA from literature reports [31–35].

For $TiO_2$–4-MBA system, the charge transfer process follows the previously reported CT mechanism of semiconductor-to-molecule [36]. In short, the electrons in the VB of $TiO_2$ (−6.49 eV) are excited to the $E_{ss}$ of $TiO_2$ (−4.53 eV to −4.57 eV) by excitation energy (1.96 eV), and then injected into LUMO of 4-MBA molecules (−2.82 eV). For the CuO-4-MBA system, the excitation energy (1.96 eV) neither meets the energy requirement for CT from HOMO of 4-MBA (−7.41 eV) to CB of CuO (−4.96 eV), nor meets the energy requirement for CT from VB of CuO (−6.66 eV) to LUMO of 4-MBA (−2.82 eV). And photoexcited electrons in CB of CuO also cannot be further transferred to LUMO of 4-MBA due to the mismatch in energy. According to the expression of polarizability tensor for Raman enhancement in semiconductor-molecule system proposed

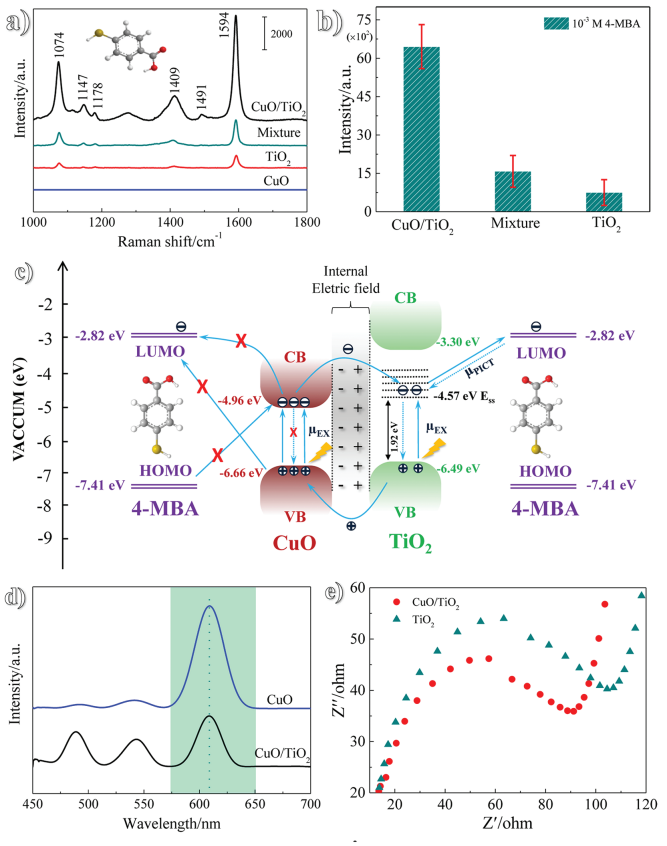


**Fig. 2.** (a) SERS spectra of 4-MBA ($10^{-3}$ mol/L) adsorbed on the surface of pure $TiO_2$, pure CuO, mixture of $TiO_2$ and CuO, $CuO/TiO_2$ heterojunction. (b) SERS intensity of the band at 1594 $cm^{-1}$ for the different substrate. (c) Proposed SERS enhancement mechanism for the PICT process in $CuO/TiO_2$–4-MBA system. (d) PL spectra of CuO and $CuO/TiO_2$ heterojunction. (e) EIS Nyquist plots of $TiO_2$ and $CuO/TiO_2$ heterojunction.

by Lombardi: $\alpha = A + B + C$, term A only allows the existence of totally symmetric Raman lines, which can rarely be observed in SERS spectra. The items B and C are the contributions from molecule-to-semiconductor and semiconductor-to-molecule charge transfer transitions, respectively [37]. Obviously, items B and C cannot be implemented for CuO-4-MBA system. Therefore, the Raman signal of 4-MBA on CuO is not enhanced.

However, when p-type semiconductor and n-type semiconductor are combined to form the heterojunction, the electrons will be transferred from the n-type semiconductor to the p-type semiconductor due to the offset of Fermi levels. Consequently, the side of n-type semiconductor is positively charged, while the side of p-type semiconductor is negatively charged. This means that an IEF will be formed at the interface of the heterojunction [38–42]. Just due to drive of the IEF, photoexcited electrons of CuO in the heterojunction can be transferred to $E_{ss}$ of $TiO_2$. In this process, CuO plays a role similar to "electron capsule" to provide additional electrons to LUMO of 4-MBA by "bridge" ($E_{ss}$ of $TiO_2$). Thus, the additional charge transfer provided by CuO effectively enhances the PICT efficiency in $CuO/TiO_2$–4-MBA system. Obviously, the additional PICT in this system depends on the strong interfacial coupling in the heterojunction. As shown in Fig. 2a, the SERS performance of the mixture of $TiO_2$ and CuO NPs is much less than that of $CuO/TiO_2$ heterojunction, which strongly demonstrates that the strong interfacial coupling in the p-n junction is crucial for the enhanced SERS performance of the substrate.

And also, it is particularly worth mentioning that strong interfacial coupling in heterojunction can not only enhance PICT but also

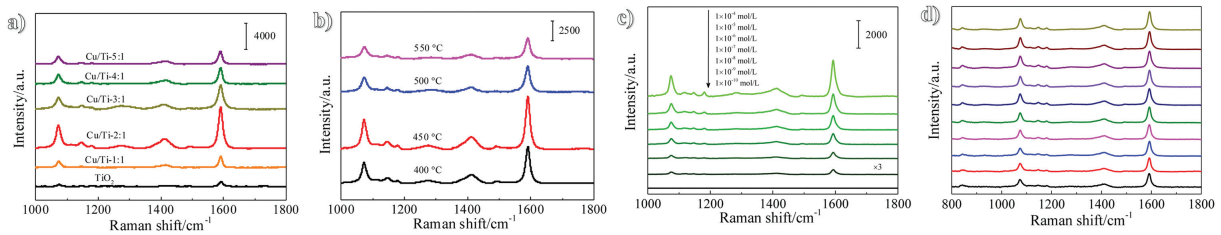


**Fig. 3.** SERS spectra of 4-MBA adsorbed on $CuO/TiO_2$ heterojunctions with (a) different Cu/Ti molar ratios and (b) different calcined temperatures. (c) SERS spectra of 4-MBA with different concentrations adsorbed on $CuO/TiO_2$ heterojunction. (d) SERS spectra of 4-MBA adsorbed on $CuO/TiO_2$ heterojunctions from 10 random measurement sites.

improve the photogenerated carrier separation. It can be confirmed by photoluminescence (PL) measurements (Fig. 2d). The PL peak of CuO at 570–652 nm (*i.e.*, green region) can be ascribed to band edge emissions that result from the recombination of electrons and holes. Compared with the luminescence intensity of CuO at 570–652 nm, the luminescence intensity of $CuO/TiO_2$ heterojunction is significantly reduced, which should be derived from improvement of the photogenerated carrier separation efficiency of CuO in heterojunction due to the strong interfacial coupling effect.

To better reveal the electron-transfer property in the $CuO/TiO_2$ heterojunction, the electrochemical impedance spectroscopy (EIS) measurements were carried out. Fig. 2e shows the typical EIS Nyquist plots of $TiO_2$ and $CuO/TiO_2$ heterojunction. The heterojunction composite has the smaller Nyquist plot diameter compared to pure $TiO_2$, which confirms that the formation of the heterojunction results in better charge separation and efficient electron transfer. Therefore, the enhanced charge collection and improved carrier separation in this system are jointly responsible for the boosted SERS performance of the heterojunction.

In order to explore the contribution of CT to SERS enhancement in $CuO/TiO_2$ heterojunction, the concept of the "degree of CT ($\rho_{CT}$)" proposed by Lombardi *et al.* [37] was used in this work (see Supporting information for specific calculation details). The calculated $\rho_{CT}$ (0.58) of $CuO/TiO_2$ heterojunction is 1.34 times higher than that (0.43) of $TiO_2$. This further confirms that the enhanced charge collection and improved carrier separation derived from the heterojunction interface can effectively enhance and promote PICT.

Since the strong SERS performance depends on effective interfacial coupling, the molar ratio of Cu/Ti in heterojunction should have an important effect on the SERS performance of the substrate. The Cu/Ti molar ratio-dependent SERS measurement was carried out in this study. As shown in Fig. 3a, when the molar ratio of Cu/Ti is 2:1, the heterojunction substrate exhibits the strongest SERS enhancement for 4-MBA probe. When the Cu/Ti molar ratio exceeds 2:1, the SERS signals of 4-MBA start to attenuate. This can be explained by the fact that the adsorption sites on the $TiO_2$ surface would be overly covered due to the excess intruoduction of CuO. Moreover, the calcination temperature of heterojunction substrate also has an effect on the SERS performance of the substrate. It can be seen from Fig. 3b that the SERS signal intensity of 4-MBA increase firstly and then decrease evidently with the increasing of calcination temperature. When the calcination temperature is 450 °C, the heterojunction substrate exhibits the greatest enhancement effect for 4-MBA probe molecule.

Next, the substrate prepared under the optimal conditions is chosen for estimating the SERS performance. As shown in Fig. 3c, the Raman signals are still discernible even when the concentration of 4-MBA reach to $10^{-10}$ mol/L. The EF of heterojunction substrate is $8.87 \times 10^6$, which is 8.61 times that of pure $TiO_2$ (see Supporting information for specific calculation details and Fig. S2 in Supporting information). As far as we know, this is the highest SERS performance among the present reported semiconductor substrate with 4-MBA (a typical non-resonant molecule) as probe (Table S2 in Supporting information), which is even comparable to precious metal substrates and those with resonant molecule as probe. In addition, $CuO/TiO_2$ heterostructure substrate also shows excellent the reproducibility. As shown in Fig. 3d, the SERS spectra intensities of 4-MBA on the heterostructure that collected from 10 random measurement sites are almost identical.

To sum up, we have successfully developed a new p-n semiconductor heterojunction ($CuO/TiO_2$) SERS substrate by sol-hydrothermal method, which can effectively boost the Raman signal of 4-MBA. The enhanced charge collection capacity and the improved carrier separation efficiency in p-n heterojunction can effectively enhance and promote PICT. The LOD of 4-MBA probe is as low as $1 \times 10^{-10}$ mol/L and the EF can reach to $8.87 \times 10^6$. This work will provide a new idea based on the interface engineering strategy for design and construction of high-performance semiconductor SERS substrate.

## Declaration of competing interest

We declare that we have no financial and personal relationships with other people or organizations that can inappropriately influence our work.

## Acknowledgments

The research was supported by National Natural Science Foundation of China (Nos. 21804054, 21773080), Natural Science Foundation of Heilongjiang Province of China for Distinguished Young Scholars (No. JQ2019B002), Excellent Discipline Team Project of Jiamusi University (No. JDXKTD-2019007), and Open Project of State Key Laboratory of Supramolecular Structure and Materials (No. sklssm2021026).

## Supplementary materials

Supplementary material associated with this article can be found, in the online version, at doi:10.1016/j.cclet.2022.107771.

## References

[1] I. Alessandri, J.R. Lombardi, Chem. Rev. 116 (2016) 14921–14981.
[2] L.J. Xu, C. Zong, X.S. Zheng, et al., Anal. Chem. 86 (2014) 2238–2245.
[3] Y.J. Lai, L.J. Dong, R. Liu, et al., Chin. Chem. Lett. 31 (2020) 2437–2441.
[4] G.R. Wu, W.S. Li, W.J. Du, et al., Chin. Chem. Lett. 33 (2022) 519–522.
[5] C.G. Qiu, Z.Y. Cheng, C.Z. Lv, R. Wang, F.B. Yu, Chin. Chem. Lett. 32 (2021) 2369–2379.
[6] Y.S. Peng, C.L. Lin, Y.Y. Li, et al., Matter 5 (2022) 694–709.
[7] Z.A. Zhou, X.H. Bai, et al., Chin. Chem. Lett. 32 (2021) 1497–1501.
[8] H. Li, Q. Zhang, C.C.R. Yap, et al., Adv. Func. Mater. 22 (2012) 1385–1390.
[9] Z.H. Zheng, S. Cong, W.B. Gong, et al., Nat. Commun. 8 (2017) 1993.
[10] Prateek Samriti, M.C. Joshi, R.K. Gupta, J. Prakash, Mater. Chem. Phys. 278 (2022) 125642.
[11] V.Rajput Samriti, R.K. Gupta, J. Prakash, J. Mater. Chem. C 10 (2021) 73–95.
[12] I. Alessandri, J. Am. Chem. Soc. 135 (2013) 5541–5544.
[13] J.R. Lombardi, R.L. Birke, J. Phy. Chem. C 118 (2014) 11120–11130.
[14] S. Cong, Y.Y. Yuan, Z.G. Chen, et al., Nat. Commun. 6 (2015) 7800.
[15] G. Song, W.B. Gong, S. Cong, Z.G. Zhao, Angew. Chem. Int. Ed. 60 (2021) 5505–5511.
[16] X.T. Wang, W.X. Shi, S.X. Wang, et al., J. Am. Chem. Soc. 141 (2019) 5856–5862.
[17] L.B. Yang, Y. Zhang, W.D. Ruan, et al., J. Raman Spectrosc. 41 (2010) 721–726.

[18] L.B. Yang, X.Y. Qin, M.D. Gong, et al., Spectrochim. Acta A 123 (2014) 224–229.
[19] L.B. Yang, Q.Q. Sang, J. Du, et al., Phys. Chem. Chem. Phys. 20 (2018) 15149–15157.
[20] J. Li, H.Z. Zhang, D.X. Yu, et al., Spectrochim. Acta A 281 (2022) 121643.
[21] Z. Huang, X.R.Wang Ariando, et al., Adv. Mater. 30 (2018) 1802439.
[22] J. Wu, P. Huang, H.T. Fan, G. Wang, W.S. Liu, ACS Appl. Mater. Interfaces 12 (2020) 30304–30312.
[23] H. Du, Y.N. Liu, C.C. Shen, A.W. Xu, Chin. J. Catal. 38 (2017) 1295–1306.
[24] L. Pan, S.B. Wang, J.W. Xie, Nano Energy 28 (2016) 296–303.
[25] D.N. Joshi, R.A. Prasath, Mater. Today: Proc. 3 (2016) 2413–2421.
[26] L. Yang, X. Li, Z.R. Wang, Y. Shen, M. Liu, Appl. Surf. Sci. 420 (2017) 346–354.
[27] M.S. Aguilar, R. Esparza, G.J. Rosas, Solid State Chem. 277 (2019) 46–53.
[28] R. Lopez, R. Gomez, M.E. Llanos, Catal. Today 148 (2009) 103–108.
[29] J. Bandara, C.P.K. Udawatta, C.S.K. Rajapakse, Photochem. Photobiol. Sci. 4 (2005) 857.
[30] S.J.A. Moniz, J.W. Tang, ChemCatChem 7 (2015) 1659–1667.
[31] L. Guo, Z. Mao, C. Ma, et al., Appl. Nano Mater. 4 (2021) 381–388.
[32] J.J. Liu, B. Cheng, J.G. Yu, Phys. Chem. Chem. Phys. 18 (2016) 115904.
[33] X.Y. Pan, M.Q. Yang, X.Z. Fu, N. Zhang, Y.J. Xu, Nanoscale 5 (2013) 3601–3614.
[34] J.W. Cui, G.H. Wang, W. Liu, et al., Fuel 290 (2021) 120066.
[35] J.H. Ran, H.B. Chen, X. Bai, et al., Appl. Surf. Sci. 493 (2019) 1167–1176.
[36] L.B. Yang, X. Jiang, W.D. Ruan, et al., J. Phys. Chem. C 112 (2008) 20095–20098.
[37] J.R. Lombardi, R.L. Birke, Acc. Chem. Res. 42 (2009) 734–742.
[38] Y.L. Tian, B.B. Chang, J. Fu, et al., J. Solid State Chem. 212 (2014) 1–6.
[39] S. Yin, J. Di, M. Li, et al., J. Mater. Sci. 51 (2016) 4769–4777.
[40] G.G. Liu, G.X. Zhao, W. Zhou, et al., Adv. Funct. Mater. 26 (2016) 6822–6829.
[41] D.L. Jiang, L.L. Chen, J.J. Zhu, et al., Dalton Trans. 42 (2013) 15726.
[42] X.J. Zhang, L. Wang, Q.C. Du, et al., J. Colloid Interface Sci. 464 (2016) 89–95.